J. Anat. (2006) **209**, pp311–320 doi: 10.1111/j.1469-7580.2006.00615.x

Functional anatomy of interhemispheric cortical connections in the human brain

Mojtaba Zarei,[1] Heidi Johansen-Berg,[1] Steve Smith,[1] Olga Ciccarelli,[2] Alan J. Thompson[2] and Paul M. Matthews[1]

[1]*Oxford Centre for Functional MRI of the Brain, Department of Clinical Neurology, University of Oxford, John Radcliffe Hospital, Oxford, UK*
[2]*Department of Headache, Brain Injury and Neurorehabilitation, Institute of Neurology, University College London, UK*

Abstract

Interhemsipheric interaction between the human cerebral hemispheres is served by abundant white-matter fibres in the human corpus callosum (CC). Damage to these fibres has notable behavioural and cognitive sequelae that depend on the exact location of the fibre loss. Until now, correlations between fibre loss and neurological disorders have been limited to post-mortem studies. Here we used probabilistic diffusion magnetic resonance imaging tractography to produce a two-dimensional map of the CC in the mid-sagittal plane. We observed an antero-posterior topography of interhemispheric tracts within the CC, consistent with our current neuroanatomical understanding of post-mortem studies in human. Callosal tract to the left and right hemispheres had comparable volume. Gender, a factor that is often reported to affect CC shape and geometry, also had no effect on the volume of the tracts. Our map showed high consistency across individuals. We propose that this map might be useful in the study of the effects of damage to human CC in neurodegenerative and cognitive disorders.

Key words anatomy; diffusion tensor imaging; human corpus callosum; mapping; tractography.

Introduction

The human corpus callosum (CC) is a crucial structure providing interhemispheric communication between the hemispheres of the brain (Schuz & Preissl, 1996). For example, transhemispheric inhibitory fibres, located in the posterior part of the CC, have an important role in complex bimanual function (Meyer et al. 1998). Although its congenital absence can apparently be asymptomatic, many studies have shown a correlation between anatomical changes within the CC and neuropsychiatric disorders (Wang et al. 1992; Hynd et al. 1995; Woodruff et al. 1995; Devinsky & Laff, 2003), dementias (Lyoo et al. 1997; Yamauchi et al. 2000; Hensel et al. 2002), multiple sclerosis (Evangelou et al. 2000; Hasan et al. 2005), motor neurone disease (Yamauchi et al. 1995) and language disorders (Preis et al. 2000; Westerhausen et al. 2005). Variation in callosal anatomy in the healthy brain can be related to gender difference (Witelson, 1989) and handedness (Witelson, 1985, 1989; Witelson & Goldsmith, 1991),

In order to study the anatomy of the CC, it is typically divided into smaller parts: the genu, body and splenium. More fine-grained anatomical subdivisions are based on dividing the length of the structure into five or ten equal portions (de Lacoste et al. 1985; Aboitiz et al. 1992). These studies showed that fibre sizes vary across different sections of the CC. Although useful, this partitioning does not consider specific patterns of anatomical connectivity. A population-based map of the cortical tracts with the CC would provide an anatomical partitioning of the structure that is based on connectivity. The utility of a population-based map is supported by the fact that fibre tracts within the CC preserve a topographical organization across mammalian species (Jacobson & Marcus, 1970; Pandya et al. 1971; de Lacoste et al. 1985). Available evidence suggests that the organization should be consistent across individuals (Aboitiz & Montiel, 2003). An accurate map of fibre tracts within the CC, based on *in-vivo* human connectional

Correspondence
Dr M. Zarei, Oxford Centre for Functional MRI of the Brain, Department of Clinical Neurology, University of Oxford, John Radcliffe Hospital, Oxford OX3 9DU, UK. F: +44 1865 222717; E: mojtaba@fmrib.ox.ac.uk

Accepted for publication *17 May 2006*

anatomy, could be useful in clinical and cognitive studies of the function of this white matter structure in the human brain.

Diffusion imaging tractography provides a non-invasive method for visualization of white matter pathways in the human brain *in vivo* (Jones et al. 1999). For example, cortical connections with thalamus (Behrens et al. 2003b), basal ganglia (Lehericy et al. 2004), internal capsule (Zarei et al. 2004) and cerebral peduncles (Ramnani et al. 2005) have been demonstrated using diffusion tractography. This method has been previously used to visualize major fibre tracts in the human CC (Abe et al. 2004; Dougherty et al. 2005; Huang et al. 2005). In this study, we exploited probabilistic diffusion tractography with non-linear image registration (Rueckert et al. 1999) to generate a sagittal population probability map of fibre tracts within the CC. We suggest that this map may be useful in studies of the anatomical substrates of hemispheric interaction in healthy individuals as well as those with cognitive and behavioural disorders (Clarke & Zaidel, 1994; von Plessen et al. 2002).

Methods and materials

Subjects

The 11 right-handed healthy subjects (seven male, four female, ages 23–57 years) have been described previously (Behrens et al. 2003b). Informed written consent was obtained from all subjects in accordance with ethical approval from the National Hospital for Neurology and Neurosurgery and Institute of Neurology (London, UK) joint research ethics committee.

Image acquisition

The same set of brain diffusion images was used for an earlier study of the organization of the thalamus (Behrens et al. 2003b). Diffusion-weighted images were obtained using echo planar imaging on a General Electric 1.5-T Signa Horizon scanner with a standard quadrature head-coil and maximum gradient strength of 22 mT m^{-1}. The following parameters were used: 60 $\times$ 2.3 mm thick image slices, f.o.v. = 220 $\times$ 220 mm^2, matrix = 96 $\times$ 96. Images were reconstructed on a 128 $\times$ 128 matrix giving a final resolution of 1.7 $\times$ 1.7 $\times$ 2.3 mm^3.

The diffusion weighting was isotropically distributed along 54 directions (σ = 34 ms, Δ = 40 ms, *b*-value = 1150 s mm^{-2}). Six volumes with no diffusion weighting were also acquired. Cardiac gating was used to minimize artefacts from pulsatile flow of the cerebrospinal fluid. The total scan time for the DWI protocol was approximately 20 min. A high-resolution T1-weighted scan was obtained with a three-dimensional inversion recovery prepared spoiled gradient echo (IR-SPgr; f.o.v. = 310 $\times$ 155 mm^2; matrix = 256 $\times$ 128; in-plane resolution = 1.2 $\times$ 1.2 mm^2; 156 $\times$ 1.2 mm thick slices; TI = 450 ms; TR = 2 s; TE = 53 ms).

Image analysis

Image analysis was carried out using tools from FSL (FMRIB Software Library, www.fmrib.ox.ac.uk/fsl). BET was used for brain extraction of T1- and T2-weighted images. FLIRT was used to derive affine transformation matrices between diffusion, T1-weighted and standard space. Effects of eddy currents and head motion were reduced by registering all diffusion-weighted images to a non-diffusion-weighted reference image using affine registration. Analysis of diffusion images was carried out using tools from FDT (FMRIB Diffusion Toolkit). Probabilistic modelling of diffusion parameters and tractography were carried out using previously described methods (Behrens et al. 2003a). Tractography was run from seed voxels within the CC and the probability of connection between these seeds and specific cortical target masks was recorded.

Definition of seed and target masks

A seed mask of the CC for each subject was drawn manually on the exactly mid-sagittal section from fractional anisotropy (FA) maps derived from the diffusion magnetic resonance imaging (MRI) data set and registered into MNI152 standard space. In order to increase consistency of manually drawn masks of the CC, we did not include voxels with an FA value of less than 0.3. In our data, we found that plotting voxel FA values against their coordinates showed that values of less than 0.3 would not be within the CC. Cortical target masks for each individual subject were defined in each hemisphere for prefrontal, premotor, M1, S1, posterior parietal, temporal and occipital cortices. Anatomical criteria for identifying these areas were as described previously (Behrens et al. 2003b). Similar to our previous study, we used a method for extrapolating tracts across the superior longitudinal fasciculus (SLF) as described previously (Zarei et al. 2004).

Connectivity-based segmentation of the CC

Individual subject analysis

For each subject, probabilistic tractography was run from seed voxels within the CC as discussed above and the probability of connection between these seeds and specific cortical target masks was recorded. Analyses were run for targets in the left and right hemisphere separately to test the consistency of the CC parcellation on the basis of strong consistent evidence from animal studies that transcallosal fibres project to functionally equivalent brain regions in the opposite hemispheres (Tomasch, 1954). Individual subject 'hard' segmentation of the CC was carried out by classifying each CC voxel according to the unique cortical target mask with which it had the highest probability of connection. In an additional representation, clusters of voxels that connected to each cortical target mask were separately defined by thresholding at 10% of the maximum connectivity value to that target mask.

Group analysis

An inclusive group CC mask was constructed by adding all individual subject CC masks together. This group CC mask was thresholded to include only those voxels in the CC that were shared among at least 70% of the subjects. Non-linear registration (Rueckert et al. 1999) was then used to warp each slice of each individual subject's CC mask to align it with the corresponding slices in the group mask. The resulting warps were then applied to individual clusters of CC voxels connected to each cortical region to align these clusters with the group CC mask space. Hard segmentation at the group level was carried out by labelling each voxel within the group CC map by the target mask to which that voxel was most strongly connected in the greatest number of individuals.

A probabilistic group map of cortical connections in the CC was constructed by binarizing clusters of CC voxels connecting to each cortical mask for each subject (using a threshold connectivity probability value of 10%) and summing these binarized clusters across subjects. CC voxel values in the resulting group maps for each cortical target area therefore reflect the number of subjects who show dominant connections between CC voxels and the cortical target of interest. These population probability maps were thresholded to include only those voxels in which greater than 30% of the population showed connections to each cortical target area. This is an arbitrary threshold, in line with that used in previous studies (Leh et al. 2006), chosen to illustrate those tracts that are relatively common across the population.

DTI quantification

We calculated two different measures of the connected volume of the callosum to each cortical region:

1 Absolute volume: the volume of voxels in the corpus callosum mask that were connected to each cortical region.

2 Relative volume: the absolute volumes normalized by dividing the volume of the connected voxels by the volume of the target. This is expressed as a percentage and is aimed to minimize the effect of target size on the volume of connected voxels.

Absolute and relative volumes of connected voxels in the seed mask provide a simple measure of the relative representation of a cortical region.

Group comparison

We used general linear models (ANOVA with repeated measures) to assess the effects of gender, cortical targets and hemisphere on absolute and relative volume of the tracts, and also on the coordinates of voxels with highest connectivity probability.

Results

Cortical connections were successfully traced within the CC in all subjects. We found a topographic organization of tracts within the CC related to the antero-posterior location of their cortical connections (Fig. 1). Connections of the prefrontal cortex were located within the genu and anterior part of the body. Premotor cortical connections were located in the mid body region. Immediately posterior to the premotor region were M1 tracts, followed by S1 tracts. Posterior to S1 were predominantly posterior parietal cortical connections. Tracts connecting to temporal cortices occupied a considerable proportion of the splenium. The occipital tracts form the most posterior part of the splenium.

The group hard segmentation map of the CC shows a topographical organization of cortical connections in the CC (Fig. 2). This map demonstrates that there is considerable overlap between adjacent cortical tracts.

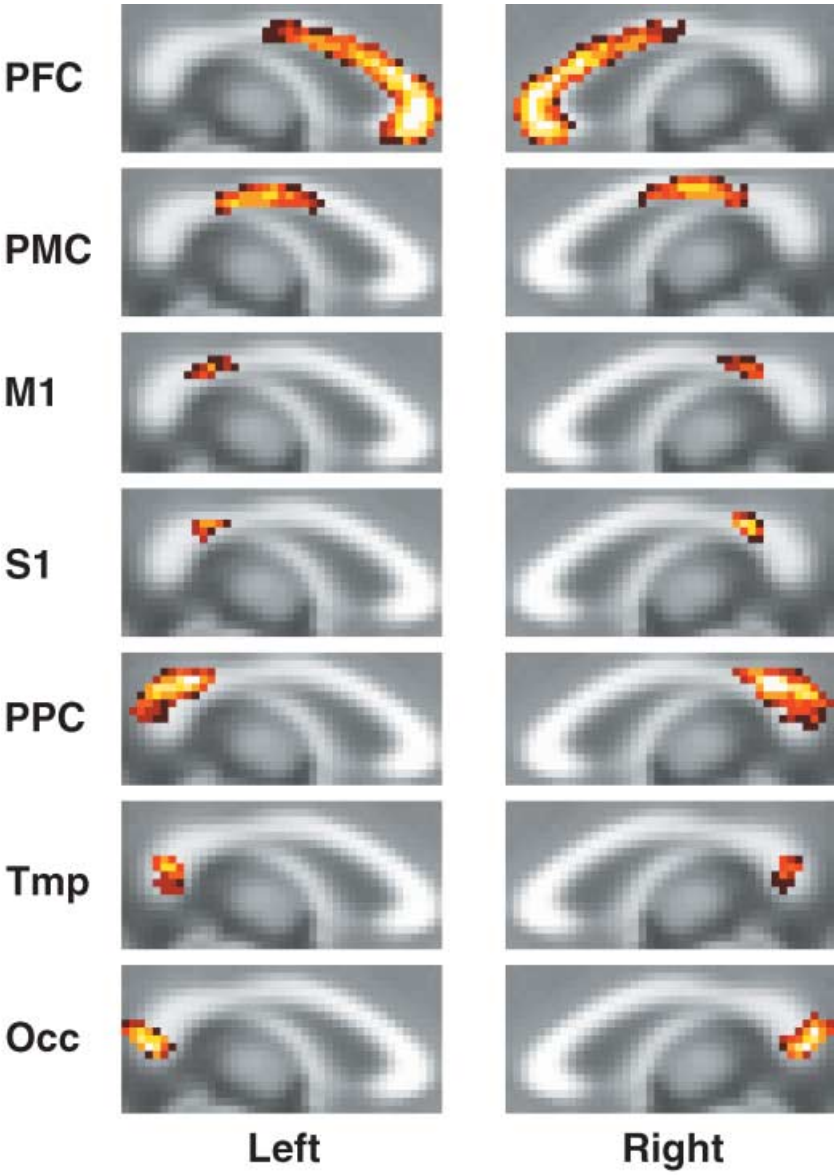

Fig. 1 Mid-sagittal group probability maps showing the location of cortical connections within the corpus callosum (CC). The organization of connections was very similar for cortical targets in the left and right hemispheres: results for tracking to cortical targets in the left hemisphere are shown in the left column, and the right hemisphere in the right column. The colour scale represents the population probability of a given CC voxel connecting to a particular target from dark red (10%) to white (100%). The map shows clear antero-posterior topographic organization. Prefrontal cortical connections occupied a large part of the volume of the CC. Abbreviations: PFC, prefrontal; M1, primary motor; S1, primary somatosensory; PPC, posterior parietal; PMC, premotor; Occ, occipital; Tmp, temporal.

This is particularly apparent between the premotor cortex and M1, and between M1 and S1 tracts (Fig. 2). The map also shows a similar organization for right and left hemisphere cortical tracts within the corpus callosum. Hard segmentation maps for individual subjects demonstrate high consistency between subjects (Fig. 3)

Reproducibility of individual measures

We tested the reproducibility of the measures by comparing connections to right and left hemispheric cortical regions. There was a high consistency of connections from CC to cortical targets in the right and left hemisphere. This was assessed by comparing the arithmetic mean in each plane as well as the geometric means of x and y coordinates for the voxels with the highest connection probability. We found a significant effect of cortical region ($F = 144.9$, $P < 0.001$), but no effect of hemisphere (Table 1).

Quantification of cortical connections

We found a significant effect of cortical region for both volume measures (absolute: $F = 123.5$, $P < 0.001$; relative: $F = 36.4$, $P < 0.001$). No effect of hemisphere was found for absolute volume, but a trend was found for the relative volumes, reflecting the tendency for greater CC volumes to be found for tracking to left vs. right

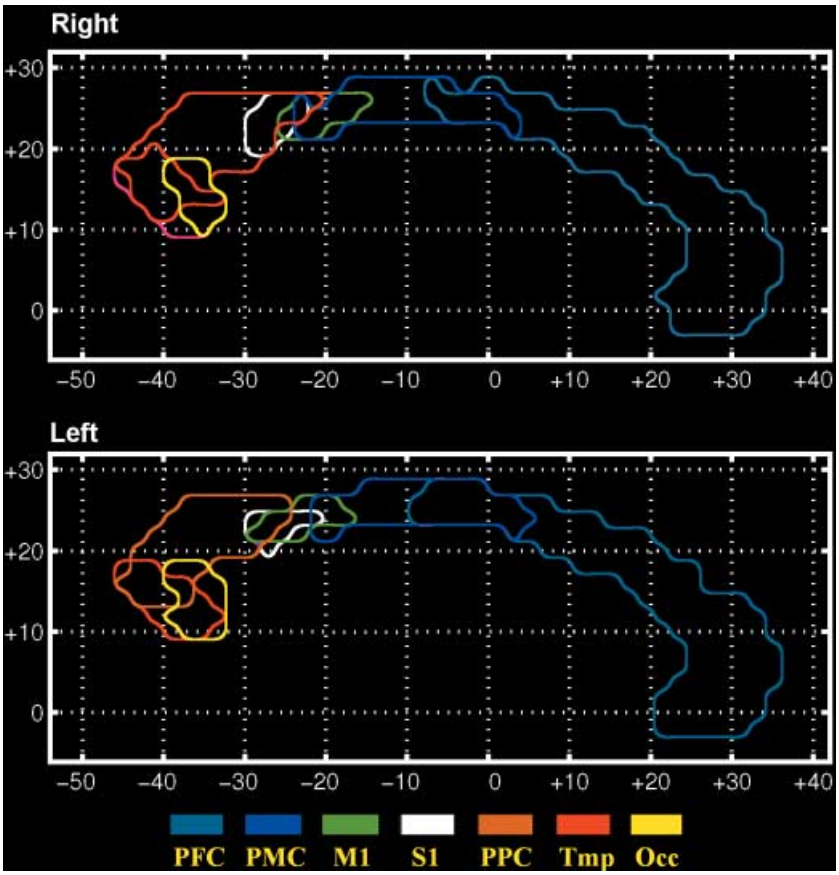

Fig. 2 Map of the corpus callosum according to the connectivity of voxels from the mid-sagittal section to seven cortical regions in each hemisphere. Results for tracking to targets in the right hemisphere are shown at the top, and for the left hemisphere at the bottom. The map demonstrates the overlap between callosal regions projecting to adjacent cortical target areas. Borders between regions are derived by thresholding the population probability maps at a probability of 30%. Abbreviations as for Fig. 1.

Table 1 Arithmetic and geometric mean of the coordinates of voxels with maximum connectivity probability to the cortical targets in standard space ($x = 0$)

	Right hemisphere			Left hemisphere		
	Arithmetic mean		Geometric mean	Arithmetic mean		Geometric mean
	$y \pm$ SEM	$z \pm$ SEM	$xy \pm$ SEM	$y \pm$ SEM	$z \pm$ SEM	$xy \pm$ SEM
M1	−23.3 ± 0.7	21.5 ± 0.3	22.4 ± 0.4	−22.7 ± 0.9	21.3 ± 0.3	22.0 ± 0.6
S1	−27.3 ± 0.5	21.3 ± 0.2	24.1 ± 0.3	−27.6 ± 0.5	20.9 ± 0.3	24.0 ± 0.4
Prefrontal	19.6 ± 2.3	7.8 ± 1.9	12.4 ± 0.6	22.7 ± 2.2	7.5 ± 1.7	13.0 ± 0.6
Premotor	−10.7 ± 1.0	23.3 ± 0.2	15.8 ± 0.5	−10.5 ± 1.4	23.1 ± 0.3	15.6 ± 0.7
Post. parietal	−37.8 ± 0.9	18.4 ± 0.7	26.4 ± 0.7	−36.4 ± 1.2	18.0 ± 0.7	25.6 ± 0.8
Occipital	−39.1 ± 0.5	10.9 ± 0.4	20.6 ± 0.2	−40.4 ± 0.5	11.3 ± 0.4	21.4 ± 0.2
Temporal	−32.2 ± 3.2	12.4 ± 1.0	20.0 ± 0.8	−31.3 ± 3.2	12.5 ± 0.9	19.8 ± 0.8

hemisphere targets ($F = 4.9$, $P = 0.05$) (Fig. 4). Gender did not have any significant effect on the absolute or relative volume of callosal tracts.

Discussion

The CC is a heterogeneous structure that is characterized by its topographic organization, connectivity of the fibre tracts and fibre tract sizes. This topography is particularly precise in primates (Lamantia & Rakic, 1990; Innocenti et al. 1995). The CC connects functionally equivalent cortical areas in each hemisphere with the exception of primary sensory and motor cortices, which are sparsely connected transcallosally (Innocenti et al. 1995). The common understanding is that the sensorimotor cortices (S1, M1 and premotor cortex) are connected

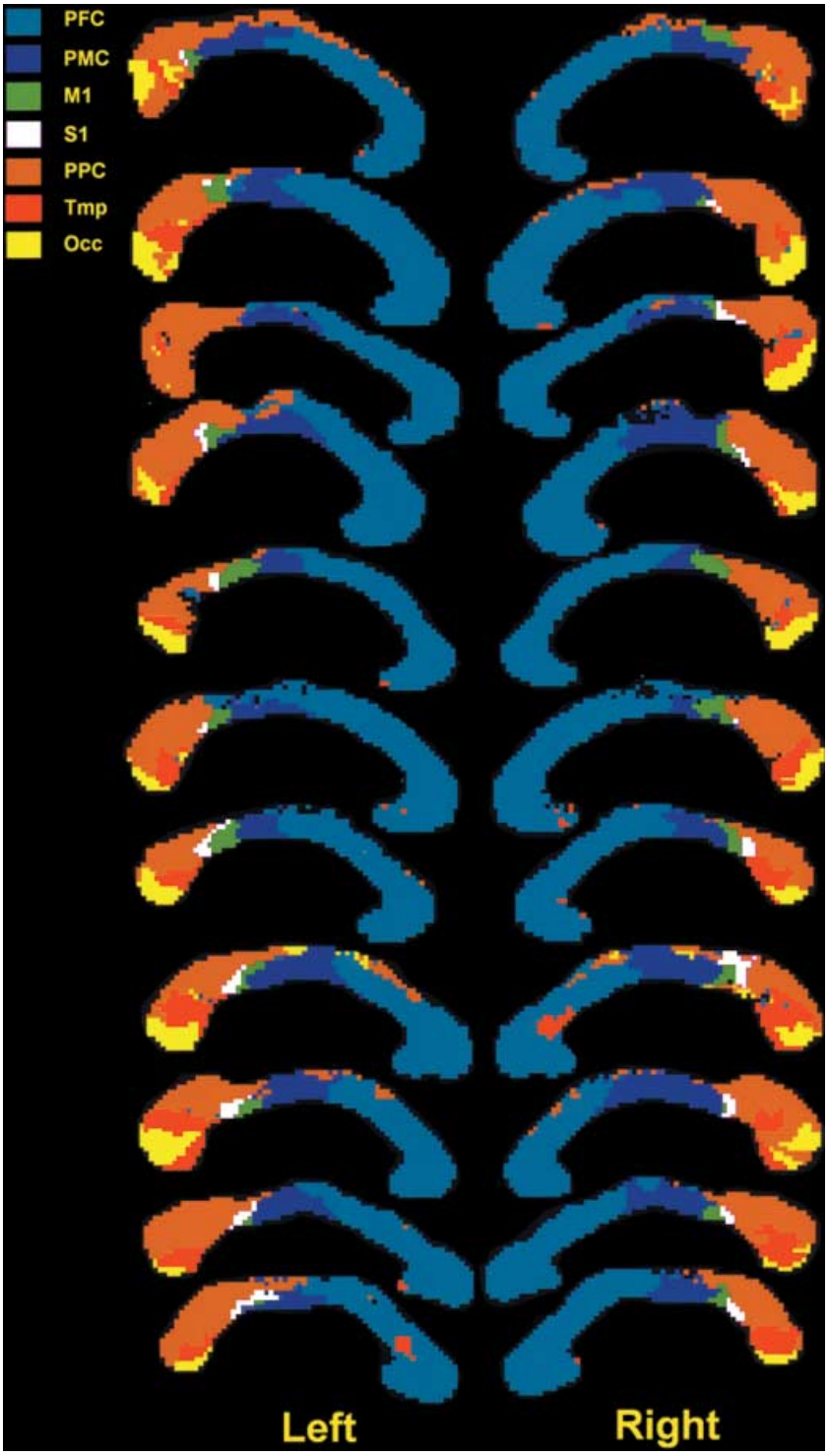

Fig. 3 Hard segmentation maps for each individual studied showing a high reproducibility and consistency across subjects and across hemispheres. Hard segmentations are created by classifying each callosal voxel according to the cortical target with which it has the highest probability of connection. Abbreviations as for Fig. 1.

monosynaptically via the CC only for areas representing the body midline area (Innocenti et al. 1995). However, there are studies that have demonstrated neurones with bilateral representation of distal limbs in monkey and rat (Iwamura et al. 1994; Zarei & Stephenson, 1996). Neurones with connections to both sides of the body are found in both hemispheres and are connected to the functionally equivalent areas of the cortex via the CC. These neurones are thought to play a role in integrative sensorimotor functions (Iwamura et al. 1994)

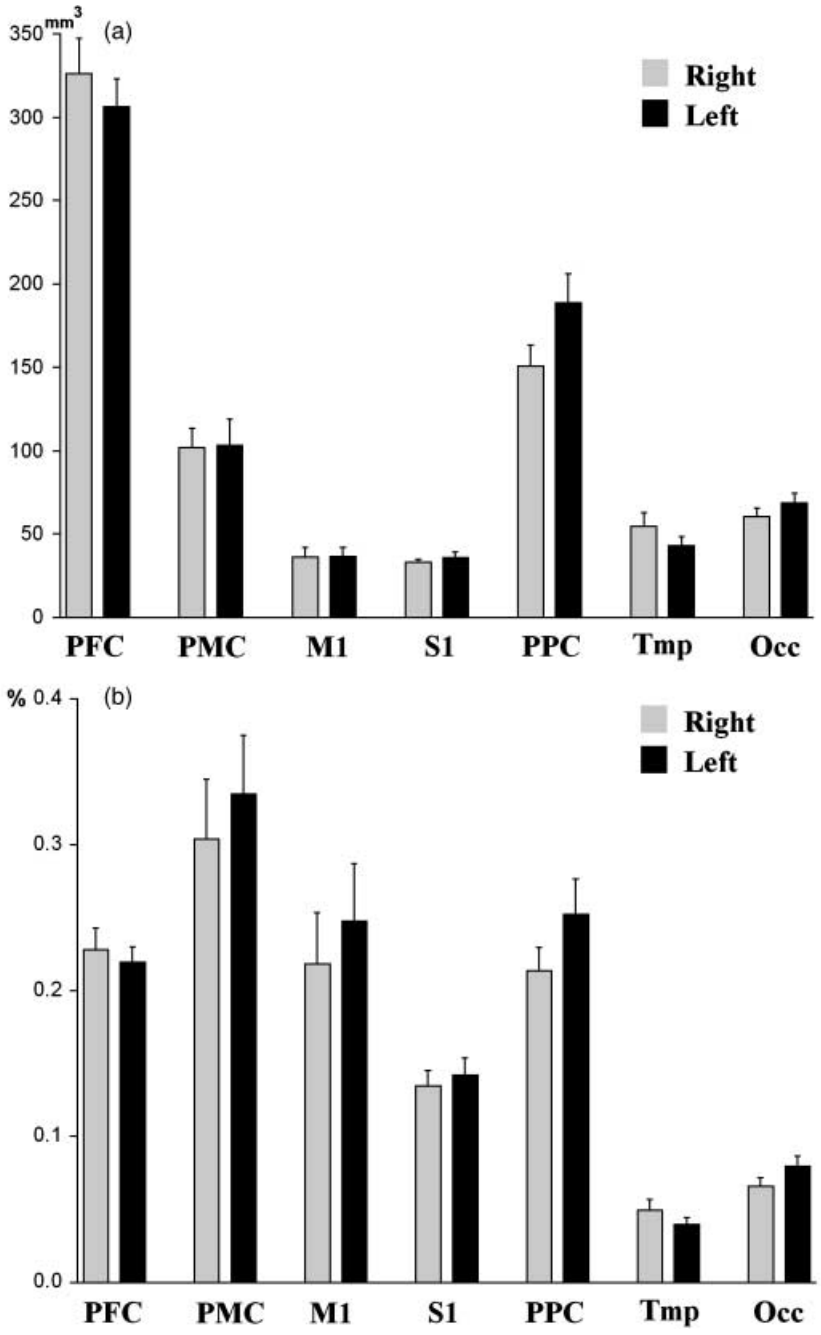

Fig. 4 Absolute (a) and relative (b) volume of callosal voxels connected to the cortical target regions. The figures show a significant effect of cortical region for both measures (absolute: $F = 123.5$, $P < 0.001$; relative: $F = 36.4$, $P < 0.001$). No effect of hemisphere was found for absolute volume, but a trend was found for the relative volumes, reflecting the tendency for greater CC volumes to be found for tracking to left vs. right hemisphere targets ($F = 4.9$, $P = 0.05$). Abbreviations as for Fig. 1.

and could explain bimanual motor performance (Eliassen et al. 1999) and mirror movements (Thut et al. 1997).

The premotor cortex (PMC) has heterotopic interhemispheric connections via the CC. In the monkey, dorsal–rostral and ventral–rostral PMC receive input from homotopic areas in the contralateral hemisphere, whereas dorsal–caudal and ventral–caudal PMC receive inputs from their homotopic area in the contralateral hemisphere as well as from dorsal–rostral and ventral–dorsal regions. In addition, the dorsal–rostral PMC receives input from prefrontal cortex (Boussaoud et al. 2005).

The prefrontal and temporoparietal visual areas are connected interhemispherically by poorly myelinated, small-diameter, slow-conducting fibres (Lamantia & Rakic, 1990; Aboitiz et al. 1992). In the rhesus monkey, commissural fibres that originate in the medial prefrontal and caudal orbital regions travel through the anterior portion of the genu and the rostrum of the CC, whereas

those from the arcuate concavity pass at the rostral border of the body of the CC (Barbas & Pandya, 1984).

Mapping human CC

We produced a two-dimensional sagittal map of the cortical tracts within the CC using probabilistic diffusion tensor imaging (DTI) tractography. The resulting map is consistent with CC fibre distributions defined in post-mortem studies (Pandya et al. 1971; de Lacoste et al. 1985). This map shows an antero-posterior topographical organization of fibres that is consistent with the topography of the cerebral cortex. Neuroantomical studies have also shown an anterior–posterior gradient within the CC based on axonal diameter, with larger fibres located more posteriorly (Aboitiz et al. 1992; Aboitiz & Montiel, 2003). For example, fibres of > 0.4 μm are predmoninant at the anterior and posterior poles of the CC but are scarce in the midbody where large fibres of > 3 μm and > 5 μm are abundant (Aboitiz et al. 1992). These large fibres connect sensorimotor cortices in each hemisphere (Lamantia & Rakic, 1990).

Our map located primary motor and somatosensory tracts in the midbody of the CC. Localization of the prefrontal connections in the genu and anterior part of the body in our map is consistent with the presence of abundant small fibres identified in this area in human post-mortem studies (Aboitiz et al. 1995) and in monkey studies (Jacobson & Trojanowski, 1977). Our map localized the posterior parietal fibres in the posterior half of the body of the CC (isthmus), similar to the findings of an autoradiographic study of this area in the monkey brain (Seltzer & Pandya, 1983). In monkey, the splenium of the CC receives fibres from the caudal two-thirds of the temporal lobe, including the temporal pole, superior and inferior temporal gyri, and parahippocampal gyrus (Demeter et al. 1990). Fibres from the occipital cortex pass through the inferior portion of the splenium in monkey (Pandya et al. 1971). A recent non-quantitative DTI tractography study on four subjects confirmed this location in human (Dougherty et al. 2005). Our map clearly shows a location of the temporal and occipital fibres with splenium that is consistent with these studies.

Production of a reliable population map of cortical connections within the CC could have useful potential clinical applications. Previously, study of the CC in cognitive and behavioural neurology has relied on parcellation schemes that cannot be applied to individuals in a precise quantitative fashion.

For example, a combined functional MRI and DTI to study the effect of cerebral dominance (and language) on relative anisotropy and mean diffusivity (Westerhausen et al. 2005) found higher relative anisotropy in the posterior third segment in the strongly left-lateralized group. This area corresponds with most sensory and motor cortical tracts in our map. The genu of individuals with dyslexia was found to be smaller than in non-dyslexics (Hynd et al. 1995). Patients with Down's syndrome were reported to have a smaller anterior one-fifth of the CC than normal subjects (Wang et al. 1992). There are reports that different types of dementia are associated with characteristic segmental atrophy of the CC. Patients with Alzheimer's disease, for example, showed a smaller posterior midbody, isthmus and splenium (Lyoo et al. 1997; Hensel et al. 2002), whereas the anterior quarter of CC is smaller in frontotemporal dementias, and patients with progressive supranuclear palsy showed atrophy of the middle–anterior quarter (Yamauchi et al. 1995, 2000). We propose that the atlas presented here may provide a useful reference guide for segmentation of the CC that can be used in clinical studies investigating the relationship between pathology and behaviour.

Limitations of the DTI and tractography used here were discussed previously (Tournier et al. 2002). Diffusion tractography cannot derive the polarity of fibre pathways. The absolute volumes of regions of connections may depend on the relative difficulty of tracking through areas of complex fibre architecture (e.g. crossing fibres). As methods for both imaging (Tuch et al. 2003) and modelling (Parker & Alexander, 2003) of complex fibre architecture develop, it will be important to test whether these new approaches confirm the organizational principles suggested here. In addition, it is important to note that the map provides information limited to cortico-cortical fibre tracts, and does not include interhemispheric connections of subcortical nuclei. A larger population of subjects would also increase the reliability of the population map produced here.

Conclusion

We have produced a probabilistic map of interhemispheric cortical pathways within the human CC using probabilistic DTI tractography. We suggest that this map may be useful in the study of neurodegenerative disorders as well as the study of interhemispheric interactions.

Acknowledgements

We are grateful to T. E. Behrens, C. F. Beckmann, C. A. Wheeler-Kingshott, P. A. Boulby, G. J. Barker, as well as to the Wellcome Trust (H.J.B.), MRC (P.M.M., H.J.B.), EPSRC (S.S.) and Department of Health (M.Z.) for funding.

References

Abe O, Masutani Y, Aoki S, et al. (2004) Topography of the human corpus callosum using diffusion tensor tractography. *J Comput Assist Tomogr* **28**, 533–539.

Aboitiz F, Scheibel AB, Fisher RS, Zaidel E (1992) Fiber composition of the human corpus callosum. *Brain Res* **598**, 143–153.

Aboitiz F, Ide A, Navarrete A, et al. (1995) The anatomical substrates for language and hemispheric specialization. *Biol Res* **28**, 45–50.

Aboitiz F, Montiel J (2003) One hundred million years of interhemispheric communication: the history of the corpus callosum. *Braz J Med Biol Res* **36**, 409–420.

Barbas H, Pandya DN (1984) Topography of commissural fibers of the prefrontal cortex in the rhesus monkey. *Exp Brain Res* **55**, 187–191.

Behrens TE, Woolrich MW, Jenkinson M, et al. (2003a) Characterization and propagation of uncertainty in diffusion-weighted MR imaging. *Magn Reson Med* **50**, 1077–1088.

Behrens TE, Johansen-Berg H, Woolrich MW, et al. (2003b) Non-invasive mapping of connections between human thalamus and cortex using diffusion imaging. *Nat Neurosci* **6**, 750–757.

Boussaoud D, Tanne-Gariepy J, Wannier T, Rouiller EM (2005) Callosal connections of dorsal versus ventral premotor areas in the macaque monkey: a multiple retrograde tracing study. *BMC Neurosci* **6**, 67.

Clarke JM, Zaidel E (1994) Anatomical–behavioral relationships: corpus callosum morphometry and hemispheric specialization. *Behav Brain Res* **64**, 185–202.

Demeter S, Rosene DL, Van Hoesen GW (1990) Fields of origin and pathways of the interhemispheric commissures in the temporal lobe of macaques. *J Comp Neurol* **302**, 29–53.

Devinsky O, Laff R (2003) Callosal lesions and behavior: history and modern concepts. *Epilepsy Behav* **4**, 607–617.

Dougherty RF, Ben-Shachar M, Bammer R, Brewer AA, Wandell BA (2005) Functional organization of human occipital-callosal fiber tracts. *Proc Natl Acad Sci USA* **102**, 7350–7355.

Eliassen JC, Baynes K, Gazzaniga MS (1999) Direction information coordinated via the posterior third of the corpus callosum during bimanual movements. *Exp Brain Res* **128**, 573–577.

Evangelou N, Konz D, Esiri MM, Smith S, Palace J, Matthews PM (2000) Regional axonal loss in the corpus callosum correlates with cerebral white matter lesion volume and distribution in multiple sclerosis. *Brain* **123**, 1845–1849.

Hasan KM, Gupta RK, Santos RM, Wolinsky JS, Narayana PA (2005) Diffusion tensor fractional anisotropy of the normal-appearing seven segments of the corpus callosum in healthy adults and relapsing-remitting multiple sclerosis patients. *J Magn Reson Imaging* **21**, 735–743.

Hensel A, Wolf H, Kruggel F, et al. (2002) Morphometry of the corpus callosum in patients with questionable and mild dementia. *J Neurol Neurosurg Psychiatry* **73**, 59–61.

Huang H, Zhang J, Jiang H, et al. (2005) DTI tractography based parcellation of white matter: application to the mid-sagittal morphology of corpus callosum. *Neuroimage* **26**, 195–205.

Hynd GW, Hall J, Novey ES, et al. (1995) Dyslexia and corpus callosum morphology. *Arch Neurol* **52**, 32–38.

Innocenti GM, Aggoun-Zouaoui D, Lehmann P (1995) Cellular aspects of callosal connections and their development. *Neuropsychologia* **33**, 961–987.

Iwamura Y, Iriki A, Tanaka M (1994) Bilateral hand representation in the postcentral somatosensory cortex. *Nature* **369**, 554–556.

Jacobson S, Marcus EM (1970) The laminar distribution of fibers of the corpus callosum: a comparative study in the rat, cat, rhesus monkey and chimpanzee. *Brain Res* **24**, 517–520.

Jacobson S, Trojanowski JQ (1977) Prefrontal granular cortex of the rhesus monkey. II. Interhemispheric cortical afferents. *Brain Res* **132**, 235–246.

Jones DK, Simmons A, Williams SC, Horsfield MA (1999) Non-invasive assessment of axonal fiber connectivity in the human brain via diffusion tensor MRI. *Magn Reson Med* **42**, 37–41.

de Lacoste MC, Kirkpatrick JB, Ross ED (1985) Topography of the human corpus callosum. *J Neuropathol Exp Neurol* **44**, 578–591.

Lamantia AS, Rakic P (1990) Cytological and quantitative characteristics of four cerebral commissures in the rhesus monkey. *J Comp Neurol* **291**, 520–537.

Leh S, Johansen-Berg H, Ptito A (2006) Unconscious Vision: New insights into the neuronal correlate of blindsight using diffusion tractography. *Brain* **129**, 1822–1832.

Lehericy S, Ducros M, Van de Moortele PF, et al. (2004) Diffusion tensor fiber tracking shows distinct corticostriatal circuits in humans. *Ann Neurol* **55**, 522–529.

Lyoo IK, Satlin A, Lee CK, Renshaw PF (1997) Regional atrophy of the corpus callosum in subjects with Alzheimer's disease and multi-infarct dementia. *Psychiatry Res* **74**, 63–72.

Meyer BU, Roricht S, Woiciechowsky C (1998) Topography of fibers in the human corpus callosum mediating interhemispheric inhibition between the motor cortices. *Ann Neurol* **43**, 360–369.

Pandya DN, Karol EA, Heilbronn D (1971) The topographical distribution of interhemispheric projections in the corpus callosum of the rhesus monkey. *Brain Res* **32**, 31–43.

Parker GJ, Alexander DC (2003) Probabilistic Monte Carlo based mapping of cerebral connections utilising whole-brain crossing fibre information. *Inf Process Med Imaging* **18**, 684–695.

von Plessen K, Lundervold A, Duta N, et al. (2002) Less developed corpus callosum in dyslexic subjects – a structural MRI study. *Neuropsychologia* **40**, 1035–1044.

Preis S, Steinmetz H, Knorr U, Jancke L (2000) Corpus callosum size in children with developmental language disorder. *Brain Res Cogn Brain Res* **10**, 37–44.

Ramnani N, Behrens TE, Johansen-Berg H, et al. (2006) The evolution of prefrontal inputs to the cortico-pontine system:

diffusion imaging evidence from Macaque monkeys and humans. *Cereb Cortex* **16**, 811–818.

Rueckert D, Sonoda LI, Hayes C, Hill DL, Leach MO, Hawkes DJ (1999) Nonrigid registration using free-form deformations: application to breast MR images. *IEEE Trans Med Imaging* **18**, 712–721.

Schuz A, Preissl H (1996) Basic connectivity of the cerebral cortex and some considerations on the corpus callosum. *Neurosci Biobehav Rev* **20**, 567–570.

Seltzer B, Pandya DN (1983) The distribution of posterior parietal fibers in the corpus callosum of the rhesus monkey. *Exp Brain Res* **49**, 147–150.

Thut G, Halsband U, Regard M, Mayer E, Leenders KL, Landis T (1997) What is the role of the corpus callosum in intermanual transfer of motor skills? A study of three cases with callosal pathology. *Exp Brain Res* **113**, 365–370.

Tomasch J (1954) Size, distribution, and number of fibres in the human corpus callosum. *Anat Rec* **119**, 119–135.

Tournier JD, Calamante F, King MD, Gadian DG, Connelly A (2002) Limitations and requirements of diffusion tensor fiber tracking: an assessment using simulations. *Magn Reson Med* **47**, 701–708.

Tuch DS, Reese TG, Wiegell MR, Wedeen VJ (2003) Diffusion MRI of complex neural architecture. *Neuron* **40**, 885–895.

Wang PP, Doherty S, Hesselink JR, Bellugi U (1992) Callosal morphology concurs with neurobehavioral and neuropathological findings in two neurodevelopmental disorders. *Arch Neurol* **49**, 407–411.

Westerhausen R, Kreuder F, Santos Sequeira SD, et al. (2006) The association of macro- and microstructure of the corpus callosum and language lateralisation. *Brain Lang* **97**, 80–90.

Witelson SF (1985) The brain connection: the corpus callosum is larger in left-handers. *Science* **229**, 665–668.

Witelson SF (1989) Hand and sex differences in the isthmus and genu of the human corpus callosum. A postmortem morphological study. *Brain* **112**, 799–835.

Witelson SF, Goldsmith CH (1991) The relationship of hand preference to anatomy of the corpus callosum in men. *Brain Res* **545**, 175–182.

Woodruff PW, McManus IC, David AS (1995) Meta-analysis of corpus callosum size in schizophrenia. *J Neurol Neurosurg Psychiatry* **58**, 457–461.

Yamauchi H, Fukuyama H, Ouchi Y, et al. (1995) Corpus callosum atrophy in amyotrophic lateral sclerosis. *J Neurol Sci* **134**, 189–196.

Yamauchi H, Fukuyama H, Nagahama Y, et al. (2000) Comparison of the pattern of atrophy of the corpus callosum in frontotemporal dementia, progressive supranuclear palsy, and Alzheimer's disease. *J Neurol Neurosurg Psychiatry* **69**, 623–629.

Zarei M, Johansen-Berg H, Ramnani N, Matthews PM (2004) In vivo mapping of cortical sensorimotor tracts in the human internal capsule. *Proceedings of the 10th Annual Meeting of the Organization of Human Brain Mapping, Budapest, Hungary*. http://www.meetingassistant.com/ohbm/meeting_plan/ohbm_mtg_index_search.php.

Zarei M, Stephenson JD (1996) Ipsilateral and bilateral receptive fields in rat primary somatosensory cortex. *Neuroreport* **7**, 647–651.